Naval Research Laboratory
Washington, DC 20375-5320

NRL/5310/MR—2021/6

FDTD Analysis of the Ultrawideband Performance of Flared-Horn Antennas

MARK KRAGALOTT
MICHAEL S. KLUSKENS

Radar Analysis Branch
Radar Division

June 3, 2021

REPORT DOCUMENTATION PAGE

Form Approved
OMB No. 0704-0188

1. REPORT DATE *(DD-MM-YYYY)*	**2. REPORT TYPE**	**3. DATES COVERED** *(From - To)*
03-06-2021	NRL Memorandum Report	Oct 2018 – Aug 2019

4. TITLE AND SUBTITLE

FDTD Analysis of the Ultrawideband Performance of Flared-Horn Antennas

5a. CONTRACT NUMBER

5b. GRANT NUMBER

5c. PROGRAM ELEMENT NUMBER
PE-62271N

6. AUTHOR(S)

Mark Kragalott and Michael S. Kluskens

5d. PROJECT NUMBER

5e. TASK NUMBER
EW-271-001

5f. WORK UNIT NUMBER
6B47

7. PERFORMING ORGANIZATION NAME(S) AND ADDRESS(ES)

Naval Research Laboratory
4555 Overlook Avenue, SW
Washington, DC 20375-5320

8. PERFORMING ORGANIZATION REPORT NUMBER

NRL/5310/MR--2021/6

9. SPONSORING / MONITORING AGENCY NAME(S) AND ADDRESS(ES)

Office of Naval Research
One Liberty Center
875 N. Randolph Street, Suite 1425
Arlington, VA 22203-1995

10. SPONSOR / MONITOR'S ACRONYM(S)

ONR

11. SPONSOR / MONITOR'S REPORT NUMBER(S)

12. DISTRIBUTION / AVAILABILITY STATEMENT

DISTRIBUTION STATEMENT A: Approved for public release; distribution is unlimited.

13. SUPPLEMENTARY NOTES

14. ABSTRACT

In this work, the FDTD technique is employed to analyze and improve the UWB pulse performance of flared-horn antennas. The transverse feed and the inline-balun feed are compared as methods of transitioning from coaxial transmission lines to parallel plates, and flared-horns fed with the inline-balun are found to have superior UWB performance. The radiation characteristics of standard flare-taper functions such as the linear taper are compared with taper functions that curl behind from the aperture plane. Untreated aperture discontinuities present standard taper functions constrain UWB radiation performance. By contrast, the tapered-back flare functions provide enhanced UWB performance primarily through the avoidance of the sharp aperture discontinuities. UWB radiation performance improves as the flare length is increased from one-quarterwavelength at the lowestUWBfrequency to lengths exceeding onehalf wavelength, albeit with a decreasing rate of performance improvement. As the aperture size grows from one-quarter wavelength at the lowest UWB frequency to one wavelength, UWB pulse radiation performance is enhanced, again with a decreasing rate of performance improvement. E-plane energy pattern symmetry can be improved by thickening or widening the plates in the flare region, or by increasing the flare length or aperture size. Finally, the array behavior of one of the tapered-back elements fed with the inline balun is studied with a waveguide simulator, and the VSWR is shown to be very low across the bandwidth.

15. SUBJECT TERMS

Pulse radiation and reception
Finite-difference time-domain
Time-domain antennas
XFDTD
Ultrawideband
Signal fidelity

16. SECURITY CLASSIFICATION OF:			**17. LIMITATION OF ABSTRACT**	**18. NUMBER OF PAGES**	**19a. NAME OF RESPONSIBLE PERSON**
					Mark Kragalott
a. REPORT	**b. ABSTRACT**	**c. THIS PAGE**	U	29	**19b. TELEPHONE NUMBER** *(include area code)*
U	U	U			(202) 404-1910

Standard Form 298 (Rev. 8-98)
Prescribed by ANSI Std. Z39.18

This page intentionally left blank.

CONTENTS

FIGURES

FDTD ANALYSIS OF THE ULTRAWIDEBAND PERFORMANCE OF FLARED-HORN ANTENNAS

1. INTRODUCTION

Flared antennas are appropriate for applications in which directive energy and wideband behavior are required. Figure 1 shows a prototype linear flared-horn with the salient features. In this basic configuration, the antenna is transverse-fed by a coaxial transverse electromagnetic (TEM) mode into the parallel-plate feed region. The plates are flared out along the boresight direction of radiation, which in the present coordinate system is the x-axis.

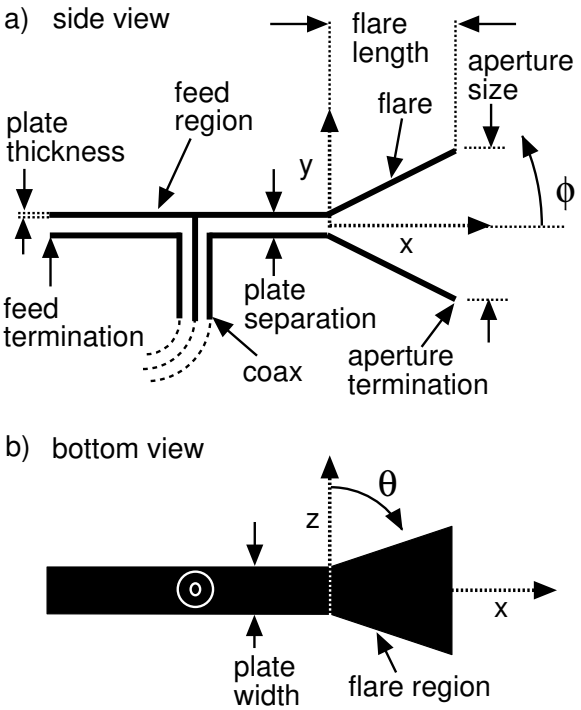

Fig. 1—The geometry of a flared horn

The primary factors that affect flared-horn radiation of an ultrawideband (UWB) signal include the waveguide modes present in the feed region, the spatial point-to-point characteristic impedance of the transmission line, the discontinuities present at the aperture and feed termination of the antenna, the flare taper shape and length, and the aperture size. The UWB pulse performance of various flared-horn configurations is investigated through a finite-difference time-domain (FDTD) [1] Maxwell equation solver. An UWB pulse is defined by a fractional bandwidth exceeding 0.25, where the fractional bandwidth is defined as the ratio of the half-power bandwidth of the signal to its center frequency. TEM horn antennas, which have a linearly

Manuscript approved June 1 2021.

expanding plate width along the flare region, are a subclass of flared-horn antennas, which, in general, can have any plate width or thickness variation in the flare region. For pulse time widths greater than the time for electromagnetic energy to traverse the flare arc-length, flared-horn antennas tend to radiate a boresight field that is a scaled replica of the derivative of the input voltage. The Carson-Rayleigh reciprocity theorem [2] states that the time-domain received response of an antenna due to an incident field $\mathbf{E}^i(t, \theta, \phi)$ will be identical to the transmitted response in the direction (θ, ϕ) if the excitation is of the form $\int_0^t \mathbf{E}^i(t, \theta, \phi)dt$. It follows that because flared-horns tend to transmit the temporal derivative of the input voltage, they also tend to receive a voltage that is a scaled replica of the incident field.

The radiation performance of good pulsed-UWB antennas is distinct from the behavior of many good conventional wideband antennas. Good UWB pulse radiators produce far-zone fields that tend to preserve the temporal shape of the input voltage pulse (or some function of it) over a preferred range of angles, whereas good conventional wideband antennas have relatively constant frequency-domain parameters including voltage standing wave ratio (VSWR), polarization, gain, and radiation pattern over the required bandwidth. In general, radiators judged to be good UWB pulse radiators also will be good conventional wideband radiators. However, good, conventional wideband antennas can have far-zone fields that severely distort the shape of an UWB pulse, rendering their performance inadequate for some UWB applications. This far-field distortion occurs if the antenna has a shifting phase center in space or time-delayed radiation of frequency components within the pulse bandwidth. Therefore, the time-domain far-fields of an antenna must be evaluated to determine whether the antenna can be classified as a good UWB pulse radiator. In this report, the time-domain far-zone and near-zone fields of various flared-horn configurations are studied, and the data can be applied to improve their UWB pulse-radiation performance. Moreover, this report provides performance data for the cornu flared horn antenna, which was designed during the research and resulted in United States patent US5973653A [3].

When antenna geometries are both complex and varied, it is convenient to employ numerical methods for the solution of their radiation characteristics [4–8]. Time-domain computational electromagnetic techniques are appropriate for the present task because they permit pulse excitation of the antenna, and thus far-zone time-domain fields are directly evaluated for UWB performance criteria including signal fidelity and energy as a function of angle. In addition, frequency-domain quantities such as reflection coefficients can be found with the application of a Fourier transform. The FDTD near-zone time-domain fields can be stored and viewed graphically as the time progression of the fields about the antenna. Simulations of this kind are a valuable analysis tool in identifying dominant radiation mechanisms. It should be mentioned that analytical techniques have been applied to tapered-slot antennas by Janaswamy [9], but the class of geometries is too limited for this study.

2. PULSE BEHAVIOR OF FLARED-HORNS

Many researchers [2, 10, 11] indicate that a perfect UWB antenna will receive or radiate a scaled replica of the input signal (or some function of the input signal without pulse-stretching) at angles not far from the far-field boresight of the antenna. The boresight is defined as the direction about which the antenna radiation performance parameters are most symmetric. At angles far from boresight, directive antennas will tend to distort the time response compared with the input signal. However, directive antennas such as flared-horns receive or radiate a large portion of the field energy at angles not far from the boresight direction, so that significant distortion off boresight does not undermine their UWB behavior.

Robertson and Morgan [11] outlined the frequency-domain characteristics necessary for the transmission of a pulse signal with no distortion. These frequency-independent characteristics include a complex conjugate match between the source impedance and the input impedance of the antenna, a constant gain over a preferred angular sector, and an effective height with a linear phase response, where the effective height is defined as the ratio of the open circuit receive voltage to the incident electric field. To receive a voltage that is a scaled replica of the incident field time-variation, an antenna should have a gain proportional to the square of the frequency as well as an effective height with a linear phase response. Because of the differing gain requirements on transmit and receive, it is not possible for an antenna element both to radiate a scaled replica of the input voltage signal and to receive a scaled replica of the incident field. It is desirable, however, to achieve predictable antenna time-domain behavior. In this paper, UWB flared-horns are designed that transmit a close approximation to the derivative of the input voltage signal and receive a voltage that is nearly a replica of the incident field.

Kraus [12] points out that it is possible to deduce the qualitative behavior of an antenna from its appearance. In particular, a flared antenna that has a twin-conductor transmission line separation much less than the highest frequency, an aperture size greater than a wavelength at the lowest frequency, a constant characteristic impedance up to the aperture, and no discontinuities will tend to have wideband characteristics. Although flared antennas are noted for wideband performance [13], a distortionless UWB receiving flared-horn is not achievable.

2.0.1 Parallel-Plate Modes

Several waveguide modes can exist in the parallel-plate feed region of the antenna depending on the geometry and source fields, although the primary mode is the TEM mode. For the TEM mode, all frequency components will propagate down the waveguide at the same velocity, so they will tend to arrive at the flare region in time synchronization. Higher-order TE_{0n} or TM_{0n} modes travel down the waveguide at velocities that vary with frequency. As a consequence, if parallel plates support TE_{0n} or TM_{0n} modes, the propagating signal will tend to distort. A parallel plate waveguide will cut off higher-order mode propagation above the wavelengths given by [10]

$$\lambda_{cutoff} = \frac{2S}{n}, \tag{1}$$

where λ_{cutoff} is the wavelength corresponding to the cutoff frequency, S is the plate separation in the same units as λ_{cutoff}, and n is the mode number. Thus, to propagate only a TEM wave, the parallel plate waveguide should have a plate separation no larger than one-half wavelength at the highest frequency component of the input signal. The width of the parallel plates sets the characteristic impedance and should be chosen for maximum or constant wideband energy transfer from the coaxial line.

2.0.2 Impedance Transitions

The antenna input impedance should remain nearly constant across the frequency band so that the individual frequency components propagate with nearly equal transmission and reflection. The impedance is defined as the ratio of the voltage to the current at a reference point along the transmission line. For reflectionless transmission, the complex conjugate input impedance of the antenna should equal the characteristic impedance of the transmission line across the bandwidth of the signal. Because the coaxial TEM transmission line has a purely real characteristic impedance, the input impedance of the antenna should be nearly real. If the antenna is treated as an extension to the transmission line, then the characteristic

impedance should transform very gradually from the coaxial line impedance to the characteristic impedance at any point along the antenna to keep wave reflections small. The initial impedance transition encountered by a propagating signal is from the coaxial line to the parallel plates. The parallel plate impedance for plates of a given thickness can be evaluated from the work of Fisk [14].

Two methods for transitioning from a coaxial line to parallel plates are the transverse feed and the inline-balun feed, as shown in Fig. 2. The transverse feed is the most popular method owing to its simplicity of construction. The transverse feed connects perpendicularly with the parallel plates and, in many UWB designs, includes a half-bicone or tuning stub at the upper plate. Electromagnetic waves emerging from the coaxial line propagate toward the aperture as well as toward the feed termination. The pulse reflecting from the feed termination will not be in time phase with the pulse traveling directly toward the aperture from the coaxial line, thus causing distortion. As a consequence, closing the parallel plates at the feed termination to mitigate backlobe radiation appears to be deleterious to UWB performance. However, if a high-impedance section is formed by an increased parallel plate separation and a short circuit at the feed termination, the larger characteristic impedance of the section relative to the parallel plate feed region will tend to force the wave toward the aperture. This approach was attempted with reasonable success in this work. The open sides of the parallel plates will permit undesirable radiation out of the plane containing the flare, although the majority of the energy propagates toward angles not far off the boresight of the antenna. Closing the plates sides is not desirable because only dispersive waveguide modes would propagate, which would cause signal distortion. When compared with the transverse feed, the most striking difference of the balun feed is its alignment along the boresight of the antenna. The inline-balun is based upon a Klopfenstein [15] impedance transition, in which a specified maximum reflection coefficient is not exceeded over the entire bandwidth with a minimum length of line. The balun was first applied by Duncan and Minerva [16] for a coax to twin-wire transition and later was applied to parallel plates by Foster [17]. The balun was applied to TEM horn designs by Foster [10] and Kolobov [18], although neither reference presented a detailed account of the antenna pulse behavior. As seen in Fig. 2, a widening slot in the outer conductor of the coax gradually increases the line characteristic impedance toward the characteristic impedance of the parallel plates. Eventually, the outer conductor is transitioned to the bottom plate and the center conductor is transitioned from a circular cross section to the top plate with super-elliptic functions. The inline orientation of the balun feed with the parallel plates reduces the amount of radiation out of the plane of the flare compared to the transverse feed. The disadvantage of the balun feed compared to the transverse feed is its complex construction. In this work, a comparison of the two coax feed methods is made, and it is seen that inline balun-fed flared-horns have much lower VSWR values and radiate pulses with less far-field signal distortion at the expense of a slightly asymmetric far-zone radiation pattern.

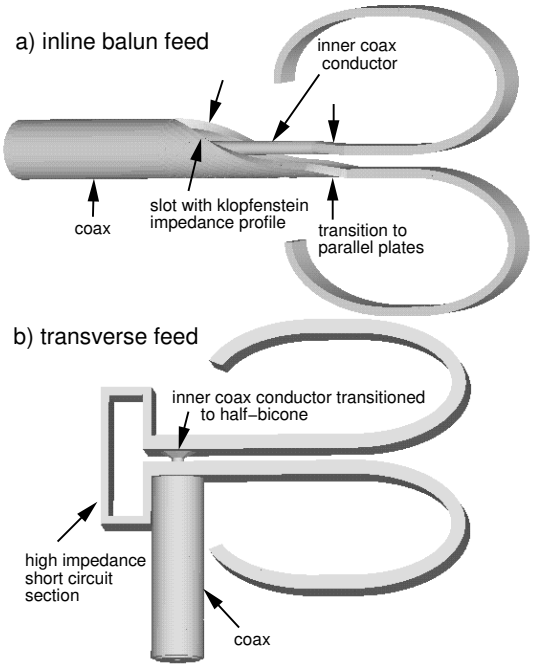

Fig. 2—(a) The inline-balun feed and (b) transverse feed shown with an elliptical taper

2.0.3 Discontinuities

Sharp geometrical features or sudden impedance changes are electromagnetic discontinuities that cause reflections and diffractions of waves. As a result, time-delayed radiation occurs and represents distortion of the far-field in relation to the input pulse. Discontinuities also increase VSWR, adversely affecting the wideband input impedance of the flared-horn. When sharp geometrical discontinuities are not avoidable, researchers have employed resistive or capacitive loading to mitigate the performance degradation, although generally dissipative losses rise with resistive loading and far-field fidelity declines with capacitive loading [19]. For example, a Wu-King resistive taper applied to monopoles [19] leads to 55 percent of the energy dissipated in heat and 21 percent of the incident energy reflected. In addition, discrete loading can be difficult to implement, expensive, and degradable. Therefore, antenna shaping should be considered the first design step, with modest applications of resistive or capacitive loading applied at the end to smooth out any performance anomalies.

2.0.4 Radiation Mechanisms and Flares

From the electromagnetic field expressions derived from the Lienard and Wiechert potentials [20], it is evident that radiation occurs because charge accelerates. Although linear charge velocity contributes to near-zone fields, these terms are inversely proportional to the square of the far-field distance, whereas the acceleration terms are inversely proportional to the far-field distance. Accelerating charge is thus the sole cause of far-field radiation. In free space, the determination of the radiated fields is trivial, but in the presence of antenna conductors, it is a complex boundary-value problem. Practical calculation of radiated fields must be performed by considering average electron accelerations together with the electromagnetic boundary conditions, and not on the complex individual electron accelerations. Consider the introduction

of a static electric field in a straight infinite conductor. Electrons accelerate under the force of the applied field and collide with the positively charged ion lattice, ultimately achieving a steady average velocity that is proportional to the electric field. Apparently, the time between no field excitation, when the average electron velocity is zero, and the achievement of the constant average electron velocity is the period that radiation occurs. Acceleration terms not only include linear acceleration, but also centripetal acceleration, which is associated with a charge traveling along a trajectory at a constant velocity but finite curvature. The acceleration a_c owing to a trajectory curvature κ and a tangential velocity v is given by

$$a_c = \kappa v^2, \tag{2}$$

where κ measures the magnitude of the derivative of the angle formed by the tangent to the the trajectory and the x-axis with respect to the parametric coordinate on the trajectory path, and is expressed in units of inverse meters. Another radiation mechanism is caused by charge accumulation at a location in the wire, such as a sharp discontinuity. Electrons incident on the location will decelerate rapidly under the repulsive forces, causing radiation. Determination of the quantitative relative contributions from each radiation mechanism is a complex task even with the most trivial geometries or field excitations and is beyond the scope of this paper. Instead, an attempt is made to isolate the effects of curvature and discontinuities to determine their impact on the UWB pulse performance of flared-horns.

As an UWB pulse fields travel down the feed region of the antenna and encounters the flare region, the induced surface charge radiates owing to the curvature of the flare. While a large portion of the energy tends to radiate in the desirable boresight direction of the flare, some of the wave energy reflects back toward the feed due to impedance changes caused by the flaring of the plates. To mitigate the the reflection, the flare-plane transition from the parallel-plate feed to the flare should be gradual.

Some UWB TEM horns are designed by maintaining a constant characteristic impedance along the linear-tapered flare region through a constant ratio between the width the plates and their separation along the flare length. The majority of the radiation occurs at the sharp aperture termination. With a constant plate-width flared-horn, the flare causes an increasing characteristic impedance with the decreasing aspect ratio of the plate width to plate separation. Linearly tapering the separation of the parallel plates without also flaring the plate width produces a sharp characteristic impedance transition at the beginning of the flare. To form a smoother impedance transition, many antenna designers employ an exponential taper [13]. Other authors [21] have synthesized the linear and exponential tapers to produce optimal tapers for a performance characteristic. Poveninelli [22] applied a Klopfenstein impedance taper to the flare, which theoretically goves a minimum taper length for a specified maximum reflection coefficient over the signal bandwidth. The linear, exponential, and Klopfenstein flares are shown in Fig. 3. Each of these designs suffers from a sharp aperture discontinuity which, for aperture sizes smaller than a wavelength, cause UWB performance degradation. The deleterious effects of the discontinuities can be mitigated to a degree if material loading or shaping of the aperture discontnuity is applied. It is recognized that many designers employ modified exponential curvatures to avoid discontinuous second derivatives at the start of the flare.

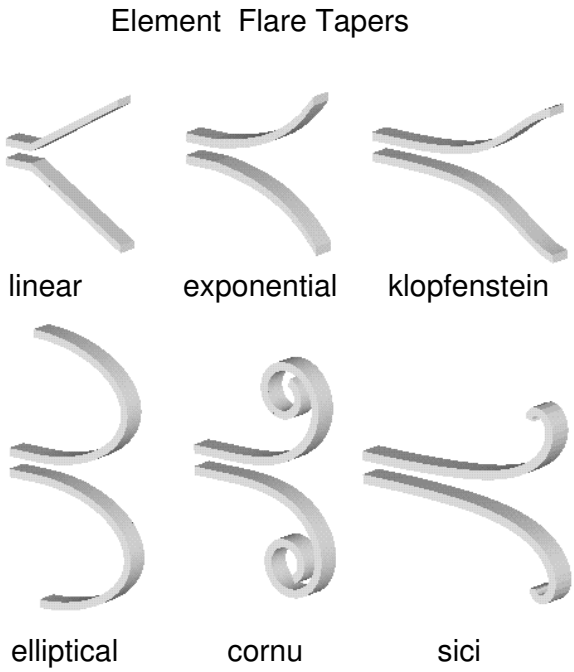

Fig. 3—The element flare tapers

Since charge acceleration due to curvature is a radiation mechanism, it is natural to study its influence on UWB radiation. In particular, flare-taper functions that avoid sharp aperture discontinuities are examined. Three such tapers are shown in Fig. 3. The elliptical taper produces a constant curvature when the ellipse degenerates to a circle. The cornu element comes from the cornu spiral [23], and it is formed by plotting the cosine fresnel integral against the sine fresnel integral. The cornu element has the property that the curvature increases linearly with the arc length. The sici element arises from the sici spiral [23], and it is formed by plotting the cosine integral against the sine integral. The sici spiral has the property of exponentially increasing curvature as a function of arc length. None of these elements has a sharp aperture discontinuity because the functions taper back from the aperture plane.

Flare length, which is defined as the distance along the boresight direction from the start of the flare to the aperture, is another geometrical feature to consider. If the flare length is at least one wavelength at the lowest frequency, then the antenna will tend to be in the traveling-wave region of operation. This region of operation allows radiation of the frequency components before encountering the aperture termination and results in less pulse distortion.

2.0.5 Aperture Size

Researchers have determined [5] that flared-horns begin significant radiation of a frequency component when the flare separation exceeds 0.4 wavelengths. Therefore, the aperture size of the antenna should be at least one-half wavelength at the longest wavelength present in the input signal. In general, apertures wider than one-half wavelength at the lowest frequency will be more efficient radiators of the low-frequency energy, but practical designs must be concerned with spatial constraints. When phase-steered arrays are designed, the element spacing at the highest frequency is required to be less than one-half wavelength to avoid

grating lobes. In such instances, it is important that the antenna radiate efficiently even when the aperture at the lowest frequency is much smaller than one-half wavelength. In this paper, a waveguide simulator example utilizing an UWB cornu element shows excellent VSWR values even with these restrictions. If the array is steered by time-delayed pulses at each element, then grating lobes, which occur at varying far-field angles with frequency, appear as low-energy-level radiation over several angles off boresight [10]. In this case, larger spacing between elements may be possible. Larger element spacings permit increased element aperture sizes conducive to good radiation efficiency at the lower frequencies, although boresight energy is reduced, owing to higher levels of off-boresight radiation.

3. FDTD ANTENNA MODELING

A standard Yee algorithm [1, 24] is employed to simulate pulse excitation of the flared-horns. Owing to the staircased approximations of the flare curvatures, an investigation into the convergence of the solution for various cell sizes is necessary. Previous research [4] has demonstrated that when modeling a smooth curvature, artificial reflections will appear if the horizontal steps of the staircased approximation to the surface are near one-half wavelength at a particular frequency. In the present research, the horizontal or vertical steps are generally much less than one-half wavelength for all of the UWB frequencies. Thiele [5] has found that in flared-horn problems, staircased algorithms are nearly as accurate as conformal algorithms when more than 33 cells per wavelength are employed. Our investigations indicate that for large curvatures in the flare region, the solution is essentially converged if 40 cells per wavelength were employed at the highest UWB pulse frequency. At the lowest UWB frequency, the resolution is 120 cells per wavelength. For a prototype flared-horn, the FDTD algorithm shows agreement to within 1 dB over most angles against the pattern calculations of a method-of-moments algorithm.

3.0.1 Coaxial feed model

For some antenna geometries [6], a single-cell FDTD coaxial-feed model is sufficient to calculate antenna performance parameters very accurately. However, in antenna problems that require very high cell resolution, there is little cost in modeling a close approximation to the physical structure of the coaxial cable. Further, the geometrical complexity of the inline balun pictured in Fig. 2 requires detailed modeling.

The FDTD modeled coaxial line is shown in Fig. 4. In the cross-sectional view of the FDTD cellular coax in Fig. 4(a), the shaded triangles represent current sources that radiate in time synchronization and have a $1/\rho$ amplitude scaling of the source function, where ρ is the the distance from the center of the inner conductor to the source location. Because the current sources mimic the electric field variation of the TEM coaxial mode, a TEM mode is set up in the coax very short distances from the excitation point. The type of FDTD source utilized is called an additive source, which means that the current source appears as a excitation current in Maxwell's equations. This type of source is advantageous in the present application because it is transparent to reflected fields passing the source location after the source amplitude is zero [25]. Energy radiated from the current sources will propagate between the conductors in both directions, although energy propagation is desired only in the direction of the antenna. The coaxial line end opposite the input of the antenna must be terminated within the FDTD space without allowing non-physical waves to reflect and become an antenna source. Thus, perfectly matched layers (PML) [26] of absorbing material are placed between the conductors near the coax termination end-cap as shown in the longitudinal cross-section depiction of the coax in Fig. 4(b). A 13-layer PML is found to reduce wave reflection in excess of 80 dB across the frequency band, which agrees well with previous waveguide results employing a PML [27].

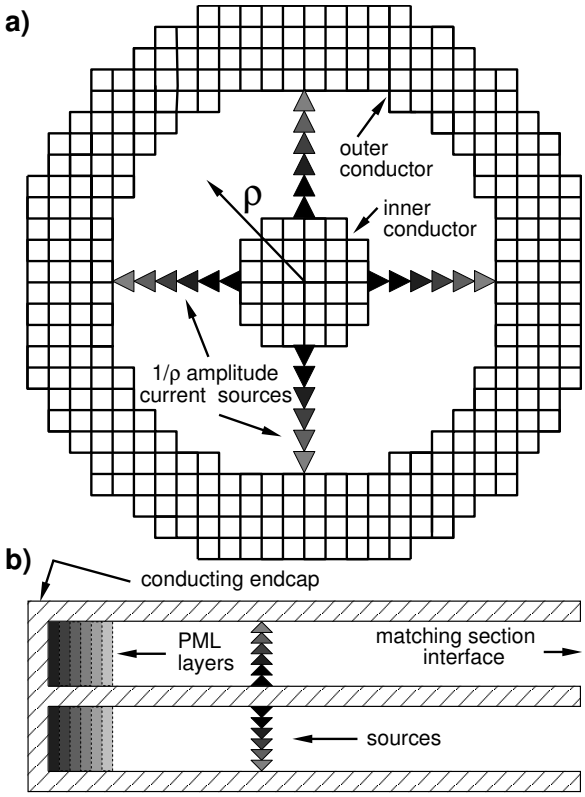

Fig. 4—The FDTD coax feed (a) transverse cross-section and (b) longitudinal cross-section

The coaxial feed is designed to support only a TEM mode at frequencies below 40 GHz. The highest frequency in the UWB pulse is 12 GHz, which corresponds to a cell size of 0.0623 cm at 40 cells per wavelength. As depicted in Fig. 4(a), the FDTD cellular cross-section of the inner and outer conductors of the coax is not perfectly circular, so it is not possible to precisely fix the characteristic impedance of the coax by selecting a ratio of inner to outer radius. Thus, it is necessary to compute the wideband characteristic impedance of the coaxial line. First, both ends of the coax are terminated with a PML, a pulse is sent down the line, and magnetic and electric field data are accumulated for all times at a reference plane. Next, the voltage at a particular time step and spatial reference plane is found from the line integral of the electric field from the inner to the outer conductor, and the current at a particular time step is determined by the closed line integral of the magnetic fields around the inner conductor. The voltage and current are Fourier transformed, and the ratio of voltage to current at a particular frequency determines the characteristic impedance. For the coaxial line shown in Fig. 4, the real part of the characteristic impedance is 56.8 ohms to within 0.03 percent from 4 to 12 GHz, and the magnitude of the imaginary part never exceeds 0.3 ohms. This flat and essentially real characteristic impedance, together with the observed $1/\rho$ variation of electric field, indicates an excellent coaxial line model.

The antenna-reflected voltage is determined by subtracting the coaxial line voltage without the antenna from the line voltage with the antenna at the reference plane. With the characteristic impedance of the coaxial line and the reflected voltage, it is a simple matter to determine both the input impedance and the VSWR of the antenna.

4. RESULTS

Lamensdorf and Susman [2] have defined performance measures for short-pulse antennas. Two of these quantities are fidelity and energy. Fidelity measures the ability of the antenna to reproduce a scaled replica of the excitation (or some function of the excitation) on receive or transmit. For a voltage $v(t)$ and the i^{th} component of field $E_i(t)$, the fidelity F is

$$\begin{aligned} F &= \max_{\tau} \int_{-\infty}^{\infty} L[\hat{v}(t)]\hat{E}_i(t+\tau)dt \\ \hat{v}(t) &= \frac{v(t)}{\sqrt{\int_{-\infty}^{\infty}|v(t)|^2 dt}} \\ \hat{E}_i(t) &= \frac{E_i(t)}{\sqrt{\int_{-\infty}^{\infty}|E_i(t)|^2 dt}}, \end{aligned} \tag{3}$$

where $\hat{v}(t)$ and $\hat{E}_i(t)$ are the voltage and field component normalized to unit energy, τ is a time variable representing cross-correlation, t is the independent time variable, $\max_\tau$ means the maximum value of the integral for all values of τ, and L is an operator. In this work, L is the derivative with respect to time on transmit, whereas on receive L is a multiplication by one. If $L[\hat{v}(t)]$ and the field component are scaled replicas of one another, the fidelity is one. Any value over 0.95 is considered to have good fidelity, whereas values over 0.98 are considered excellent. On transmit, the energy radiated $U(\theta, \phi)$ is given by

$$U(\theta,\phi) = \frac{1}{Z_0}\int_{-\infty}^{\infty} |\mathbf{E}|^2(\theta,\phi,t)dt, \tag{4}$$

where $\mathbf{E}$ is the far-zone electric field, and Z_0 is the ambient medium impedance.

The input signal is shown in Fig. 5(a). The signal is a modulated gaussian sine wave, which is given by

$$V_i(t) = A\exp(-[(t-3\tau)/\tau]^2)\sin(\omega_c[t-3\tau]), \tag{5}$$

where A is the maximum amplitude, t is the time, $\tau = 1/[\pi(f_h - f_c)]$, f_c is the center frequency of the pulse (8 GHz), f_h is the e^{-1} decay frequency point of the pulse (12 GHz), and $\omega_c = 2\pi f_c$. The lower-frequency e^{-1} voltage falloff point is 4 GHz, and the 3 dB fractional bandwidth of the signal is 60 percent. This signal is the incident electric field pulse in receive problems and the input voltage pulse in radiation problems. The base pulse-width of the signal is approximately 318 picoseconds and the signal bandwidth normalized to peak amplitude is shown in Fig. 5(c). The input signal is the reference signal for calculating fidelity for antenna reception. The current signal is a scaled replica of the voltage signal. The derivative of voltage signal shape, shown in Fig. 5(b), is the reference for calculating the fidelity of far-zone fields radiated by the antenna. Time-domain differentiation corresponds to a frequency-domain multiplication of the input voltage frequency components by $j\omega$. Thus, an antenna that produces a temporal derivative radiates a scaled product of the input voltage frequency component and frequency. For flared-horns, this translates to a lower radiation efficiency as the frequency decreases because of a decreasing aperture size in terms of wavelengths.

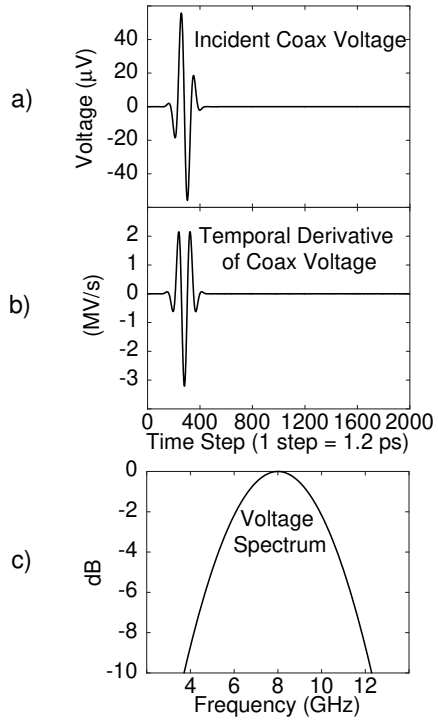

Fig. 5—(a) The incident coax voltage, (b) the temporal derivative of the coax voltage, and (c) the coax voltage spectrum

4.0.1 Transverse vs. Inline-Balun Coaxial Feeds

The initial investigations involved the manner of feeding the UWB flared-horns. The transverse coaxial feed and the inline balun feeds are shown in Fig. 2 with an elliptically tapered flared-horn attached. The elliptical taper is chosen because of the absence of sharp aperture terminations, which would complicate the comparison between the feeds because of increased reflections. The aperture size is nearly 4.1 cm, which is slightly more than one-half wavelength at the lowest UWB frequency, and the flare length is 3.4 cm. The width of the parallel plates for the transverse-fed antenna is set at 1.79 cm, and the parallel plate width of the balun-fed antenna is 0.623 cm. The parallel plate width of the inline-balun antenna is slightly larger than the inner coax diameter, but the transverse-fed antenna must have a plate width at least as wide as the outer coax diameter. The parallel plate separation for the inline balun-fed antenna is 0.3738 cm, and the separation is 0.7 cm for the transverse-fed antenna, which from Eq. (1) is sufficient to cutoff higher-order modes for both antennas. It was found that setting the parallel-plate separation of the transverse-fed antenna to 0.3738 cm to match the characteristic impedance of the coaxial line led to highly degraded VSWR and fidelity values, so the better-performing larger plate separation is selected for comparison. The plate thickness for both antennas is set at 0.25 cm. The parallel-plate length of the transverse-fed antenna is 5 cm, whereas the parallel-plate length of the balun-fed antenna is 1 cm. The backplane of the high impedance section on the transverse-fed antenna is one-quarter wavelength from the coaxial line at the center frequency, and the plate separation in this region is approximately 4 cm. The inline-balun is designed to transition from a coax impedance of 56.8 ohms to a parallel-plate impedance of 109 ohms, with a maximum reflection coefficient of 0.01 over the frequency band, which causes a balun length of approximately 5 cm. The parallel-plate separation of the flared-horn is the same as the difference of the outer and inner radii of the coaxial cable, but the separation could be made greater if the ratio of width of parallel plates to their separation is maintained after the balun section.

Figure 6(a) shows a comparison of the reflected voltage at a reference plane in the coax for the balun-fed and the transverse-fed antennas. The transverse-fed antenna has a significant reflected voltage compared with the incident voltage shown in Fig. 5(a). By contrast, the balun-fed antenna has a relatively small reflected voltage. Correspondingly, Fig. 6(b) shows a vastly inferior VSWR for the transverse-fed antenna compared with the balun-fed antenna. The lowest VSWR of the transverse-fed antenna is 1.5 at a frequency of 5.25 GHz, and has a peak VSWR of approximately 7.33 at 7.15 GHz. Other transverse-fed designs [28] demonstrate a similar peak within their designed frequency bandwidth, and a much higher VSWR off the peak compared to the in-line balun. The VSWR of the balun-fed elliptical flared-horn never exceeds 1.75 over the frequency-band, and above 6 GHz never exceeds 1.25. The VSWR can be expected to be even lower if the balun is made longer, which, with a Klopfenstein taper, implies a lower reflection coefficient over the band. The VSWR of the FDTD balun transition from coaxial line to parallel plates also is plotted, and it is seen that the VSWR remains below 1.22 across the entire band. The FDTD balun is not a precise implementation of the theoretical balun, owing to the noncircular cross section of the FDTD coax and the discrete angular cuts created in the outer conductor slot. As a consequence, the calculation understates the effectiveness of the balun, as evidenced by FDTD convergence tests that show the balun VSWR decreasing as cell size decreases.

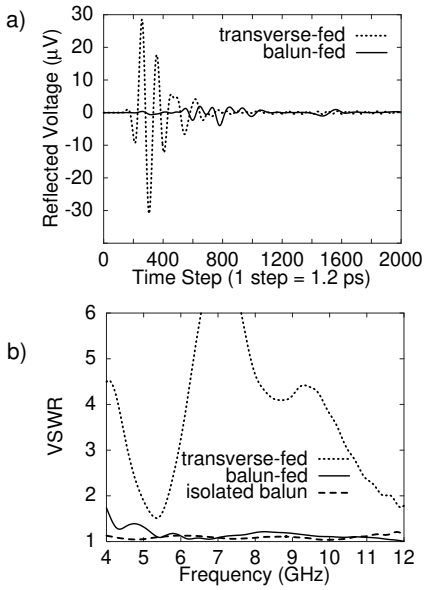

Fig. 6—The transverse-fed and balun-fed elliptical flared-horns are compared for (a) reflected voltage and (b) VSWR

Figure 7 shows the boresight (ϕ=0, θ=90) radiated ϕ-component of electric field, or co-pol, for the transverse-fed elliptical flared-horn and the co-pol radiated by the balun-fed ellipse. Although the shape of the signals is very similar from the start of each pulse to 350 time steps later, there is a considerable amount of late-time radiation from the transverse-fed antenna owing to multiple internal reflections. Further, the magnitude of the pulse peak is larger in the balun-fed antenna compared with the transverse-fed antenna. Both antennas have cross-pol peaks that are 60 dB down from the co-pol peaks.

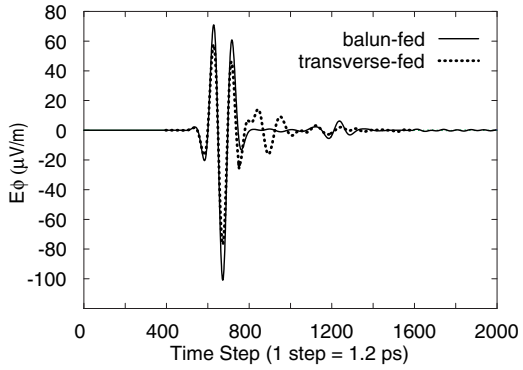

Fig. 7—The radiated ϕ-component of electric field, or co-pol, is compared for the balun-fed and transverse-fed elliptical flared-horns

Figure 8(a) shows the energy, normalized to the boresight far-field energy, of the two designs radiated in the H-plane (xz plane in Fig. 1). The inline-balun is seen to have a half-energy beamwidth of 52 degrees, whereas the transverse-fed design has a half-energy beamwidth of 36 degrees. In a array environment, large transverse radiation energy levels at $\theta = 0, \phi = 0$ lead to far-zone pulse stretching [10], and this level is considerably higher in the transverse-fed design than in the inline-balun design. The H-plane cross-pol is a significant factor in the inline-balun antenna, with a peak level of 8 dB down from the boresight co-pol at 27 degrees off boresight compared with a peak level for the transverse-fed antenna of 15 dB down at 30 degrees. Nevertheless, the wider energy pattern and lower transverse radiation of the inline-balun make it a more attractive alternative. Figure 8(b) shows the asymmetrical energy patterns in the E-plane (xy plane in Fig. 1) of the geometrically asymmetric transverse and inline feed designs. The half-energy beamwidth of each design in the E-plane is approximately 70 degrees. The large asymmetry in the energy pattern of inline-balun horn can be mitigated by increasing the width of the plates in flare region, increasing the thickness of the plates in the flare region, or increasing the flare length. In both antennas, the peak energy of the cross-pol in the E-plane is at least 50 dB down compared with the boresight energy.

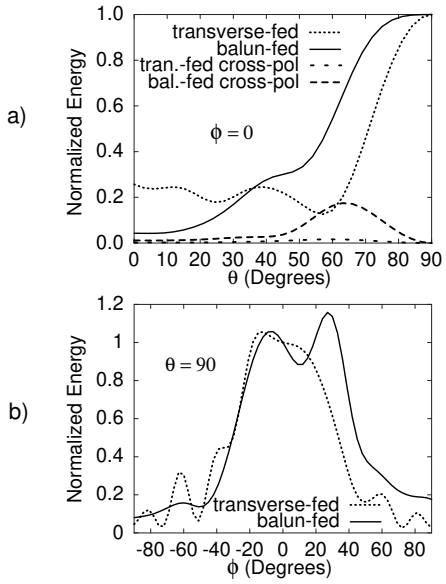

Fig. 8—The transverse-fed and balun-fed elliptical flared-horns are compared for (a) the total and cross-pol energy normalized to boresight energy in the H-plane and for (b) the total normalized energy in the E-plane

Figure 9(a) shows the fidelity compared to the derivative of the input voltage signal of each design in the H-plane, and Fig. 9(b) shows the fidelity in the E-plane. The inline-balun design has a superior far-zone fidelity over all angles for which the radiated energy is significant. As a result of the balun's superior UWB performance, all following examples employ the inline balun as a feed. It should be noted that it is possible to employ tuning stubs in the transverse-fed antenna to mitigate the peak VSWR, but such narrowband solutions could lead to degradation in performance in other frequency ranges.

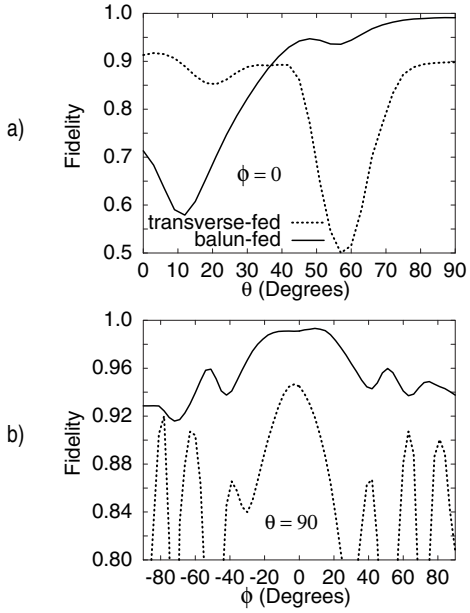

Fig. 9—The fidelity of the transverse-fed and balun-fed elliptical horns are compared for (a) H-plane fidelity and (b) E-plane fidelity

4.0.2 Effects of Discontinuities at the Aperture

From Fig. 3, it is evident that the linear, exponential, and Klopfenstein elements have sharp aperture terminations that are absent in the elliptical, cornu and sici elements. The radiation characteristics and VSWR of linear, exponential, and Klopfenstein flared-horn tapers are compared with the performance of the cornu taper. The aperture size of each element is 4.1 cm, which is slightly greater than one-half wavelength at the lowest UWB frequency of 4 GHz, and the flare length is approximately 3.4 cm. The plate width is 0.623 cm and the plate thickness is 0.25 cm.

Figure 10 shows the VSWR of the three sharp-aperture-termination elements and the cornu element. The cornu flared-horn has a significantly lower VSWR compared with any of the sharp-aperture-termination elements. The linear element has the most inferior VSWR, with a value of 3.25 at 4 GHz and a local peak value of 2.75 at 7.5 GHz. The exponential and Klopfenstein tapers have similar behavior, with a VSWR exceeding 2 below 5 GHz and a VSWR oscillating between 1.1 and 2.3 over the rest of the frequency band.

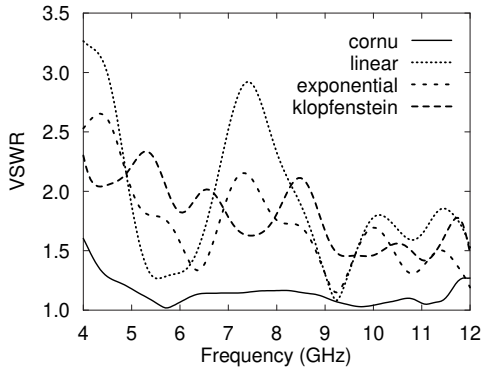

Fig. 10—Various balun-fed flare tapers are compared for VSWR

Figure 11 shows the boresight-radiated fields of the linear and cornu balun-fed flared-horns, and it is seen that the field variations closely resemble the derivative of the input voltage signal, which is shown in Fig. 5(b). The linear taper has far-field late-time radiation owing to reflection and re-radiation from sharp geometrical changes at the start of the flare and the aperture. The received voltage from the linear and cornu tapers also are shown in Fig. 11. The received voltage closely resembles a replica of the incident field variation, which is shown in Fig. 5(a). The received voltages are identical to the received voltages predicted by the time-domain reciprocity theorem.

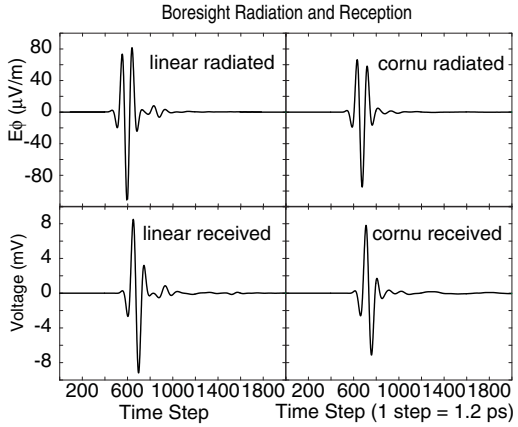

Fig. 11—The co-pol fields radiated and voltages received are plotted for the balun-fed linear and elliptical tapers

The E-plane far-field angular energy indicates a 70 degree half-energy beamwidth for the cornu taper, a 54 degree beamwidth for the exponential and Klopfenstein tapers, and a 45 degree beamwidth for the linear taper. The tapered-back cornu element provides a wider angular distribution of energy as traveling waves radiate from the gradually curved surface, whereas the sharp aperture truncation causes a more restricted energy pattern. In the H-plane, the half-energy beamwidth of the cornu and Klopfenstein elements is approximately 56 degrees, and the beamwidth of the exponential and linear elements is approximately 66 degrees.

A comparison of the radiated-field fidelity compared to the signal derivative for the four elements is shown in Fig. 12 for the E-plane. The fidelity of the sharp-termination tapers slightly exceeds that of the cornu taper (0.995) on boresight, with the Klopfenstein taper having the highest fidelity at 0.998. At angles exceeding 35 degrees off boresight, the cornu taper maintains a high signal fidelity ($\geq$ 0.94,) owing to the absence of the sharp aperture terminations, while the other three elements drop below a fidelity of 0.9. On receive, the fidelity of the voltages compared to the boresight incident field is 0.987 for the cornu taper and 0.992 for the linear taper, so both elements give an excellent reproduction of the incident field.

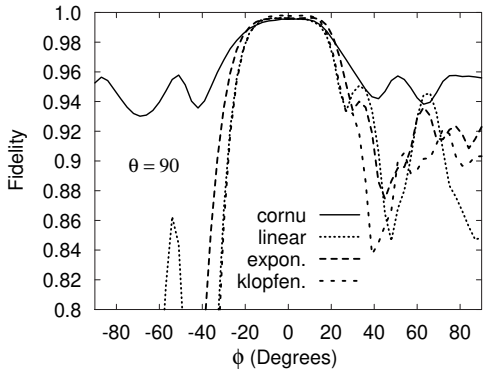

Fig. 12—The fidelities in the E-plane for various balun-fed tapers are compared

4.0.3 Effects of Flare Curvature

The acceleration of electrons owing to a curved surface causes a far-zone radiation component. It is thus natural to investigate the radiation and VSWR characteristics of elements with varied curvatures. A requirement for these tapers is the avoidance of the sharp aperture terminations, which elevate the VSWR through reflection. Figure 3 shows the three elements employed. All of the elements have an aperture size of approximately 4.1 cm. The elliptical element was degenerated into a circle to study a taper of constant curvature, whereas the cornu and sici spiral elements were employed to investigate linear and exponentially increasing curvatures, respectively, as a function of arc length. The far-field waveforms and E-plane and H-plane fidelities and energies are not significantly different from the same quantities plotted for the elliptically tapered flared-horn in Figs. 6-9 to warrant presentation here. However, the constant curvature (elliptical) and linearly increasing curvature (cornu) have slightly better fidelities than the exponentially increasing curvature (sici), and the energy patterns become slightly more directive as the taper curvatures change more rapidly with arc length. The most noticeable difference between the elements is seen in the VSWR plot in Fig. 13. The linearly increasing curvature (cornu), with a VSWR that exceeds 1.2 only at the extremities of the bandwidth, has a distinct performance advantage over the constant curvature (elliptical) or exponentially increasing (sici) curvatures, although the VSWR values for the these two elements is also very good. When compared with other UWB designs [29], the VSWR of the tapered-back, balun-fed flared-horn antenna is lower over most of the frequency band in spite of being an electrically smaller structure without loading.

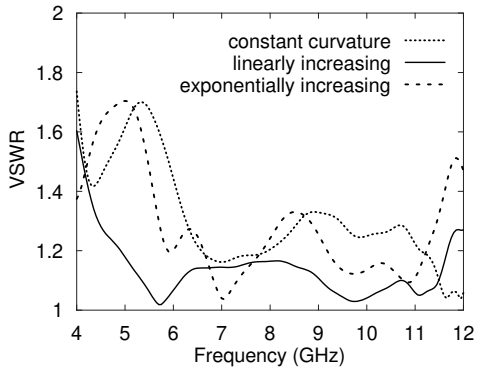

Fig. 13—The VSWR is plotted for various balun-fed taper curvatures

4.0.4 Flare Length and Aperture Size Effects

Since flare length and aperture size are determining factors in the traveling-wave character of the waves, it is interesting to study UWB performance as a function of these geometrical variables for constant width elliptical tapers. In Fig. 14(a), it is seen that with the aperture size held constant, the VSWR improves substantially as the taper length is increased from one-quarter wavelength at the lowest UWB frequency to lengths exceeding one-half wavelength, although the rate of performance improvement is decreasing in this region. In Fig. 14(b), the asymmetry of the inline-balun energy pattern in the E-plane diminishes as the flare length increases. Figure 15(a) shows that as the aperture size grows from one-quarter wavelength at the lowest UWB frequency to one wavelength, the VSWR is reduced, although with a decreasing rate of performance improvement in this region. Figure 15(b) shows that the asymmetries in the flared-horn E-plane energy pattern diminish as the aperture size increases from 2.5 cm to 4.5 cm, but then increase as the aperture size grows to 8.5 cm.

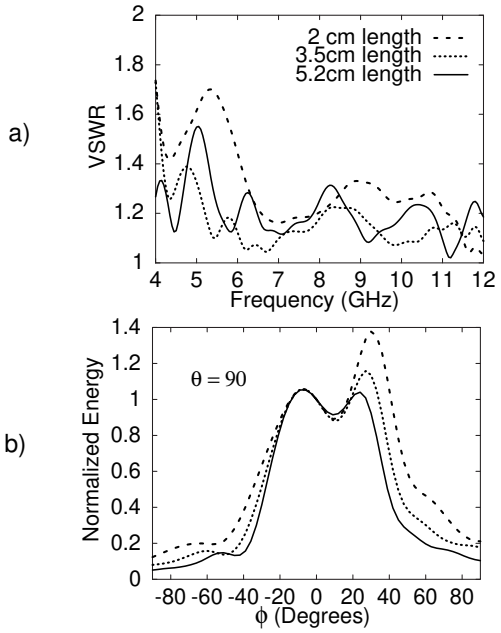

Fig. 14—The influence of flare length on elliptical flared-horn (a) VSWR and (b) E-plane energy are plotted

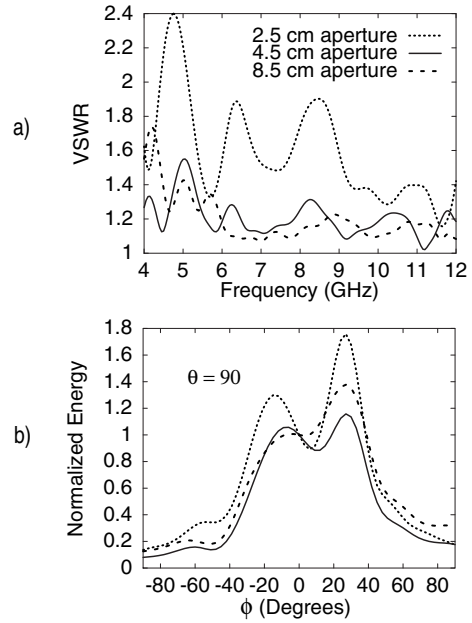

Fig. 15—The effects of aperture size on the (a) VSWR and (b) E-plane energy of a balun-fed elliptical flared-horn are plotted

4.0.5 Flare Plate Width and Thickness Effects

Thus far, all of the flared-horn geometries have had plate widths and thicknesses that are constant in the flare region. If the plate width increases in the flare region, then the antenna is similar to a TEM horn, and if the plate thickness increases and the constant plate width is relatively narrow, then the antenna is similar to a coplanar-strips antenna. Figure 16 shows an elliptically tapered TEM horn and coplanar-strips radiator together with a linearly tapered TEM horn.

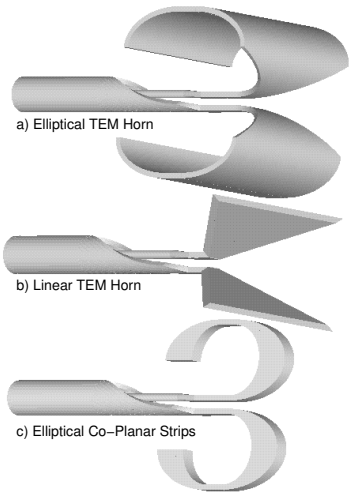

Fig. 16—(a) The elliptical TEM horn, (b) the linear TEM horn, and (c) the elliptical coplanar-strips antenna are depicted

The TEM horn considered maintains the characteristic impedance from the parallel-plate section to the aperture by keeping the ratio of plate width to separation nearly constant, and the coplanar-strips characteristic impedance in the flare region is nearly constant by keeping the ratio of the plate thickness to separation nearly constant. The E-plane taper dimensions are the same as the constant width elements in Section 4.0.2. As shown in Fig. 17(a), the E-plane energy asymmetry of the narrow constant width elements evident in Fig. 7 largely has been mitigated by the gradual widening or thickening of the plates in the flare region.

The linearly tapered TEM horn has a narrower pattern compared with the elliptically tapered elements, and the elliptical TEM horn radiates peak energy in the boresight direction. The VSWR values of the three antennas are shown in Fig. 17(b), with the linear TEM horn remaining below 1.9 across the bandwidth, the elliptical coplanar-strips staying below 1.5, and the elliptical TEM horn below 1.3, which is nearly the VSWR of the balun alone. The TEM horns are seen to provide a much wider angular H-plane fidelity compared with the source derivative than the strip or constant-width elements, although the narrower elements have an angular sector of 110 degrees for which the fidelity exceeds 0.9.

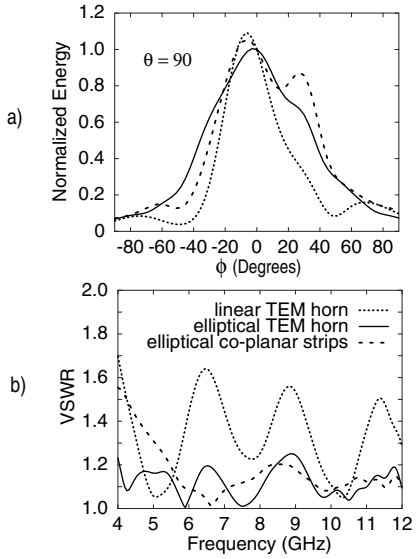

Fig. 17—The TEM horns and coplanar-strips designs are compared for (a) E-plane energy and (b) VSWR

4.0.6 Array VSWR

Finally, the broadside infinite-array VSWR characteristics are found for a balun-fed constant width cornu element with less than half-wavelength spacing at the highest frequency in the E-plane and H-plane directions. Previously, most of the elements considered have had half-wavelength apertures at the lowest UWB frequency, which enhances the low-frequency VSWR and radiation characteristics. The E-plane cornu element extent (including the spiral section) is approximately 3.8 cm, which is less than one-half wavelength at the highest frequency of 3.5 GHz. The E-plane spacing was 4.25 cm, and the H-plane spacing was 3.7 cm. Figure 18 shows the VSWR for broadside-array radiation as a function of frequency, and it is seen that from 2.8 to 3.7 GHz, the VSWR remains below 2.

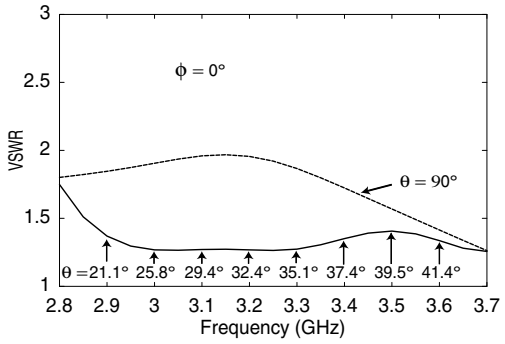

Fig. 18—The VSWR of a balun-fed cornu element array with half-wavelength spacing at 3.5 GHz is plotted for various scan angles

In addition, the VSWR of the array for particular H-plane scan angles and frequencies are plotted. As indicated in the figure, decreasing frequency in the waveguide simulator corresponds to an increasing scan angle. For all angles and frequencies indicated, the VSWR remains well below 2, and only exceeds 2 for

scan angles in excess of 70 degrees and corresponding frequencies below 2.8 GHz. The bandwidth of the array for large scan angles is estimated at 25 percent, which is just into the UWB regime.

5. SUMMARY

In this work, UWB flared-horn antennas have been evaluated and their pulse performance improved from FDTD simulations. The pulse width was slightly larger than the maximum dimension of any of the flared-horn antennas considered. The transverse feed and the inline-balun feed have been compared as UWB methods for transitioning from coaxial transmission lines to parallel plates, and it was found that antennas with the inline-balun feed have a superior VSWR and far-field pulse fidelity, although the far-field energy pattern of the balun-fed antenna was more asymmetric in the E-plane than the transverse-fed antenna. The radiation characteristics of taper flares such as the linear and exponential tapers were compared with taper functions that naturally taper back behind the aperture plane, such as the cornu tapered flared-horn. It was found that the sharp aperture discontinuities present in standard linear and exponential taper functions limit their UWB VSWR performance, although the balun feed permits high-fidelity boresight radiation by these elements. By contrast, the tapered-back functions provided excellent UWB radiation performance by the avoidance of the sharp aperture discontinuities. The curvature of the tapered-back function did not appear critical to the antenna's far-field fidelity or energy patterns, but the linearly increasing curvature, or cornu element, had an advantage in lower VSWR across the bandwidth. The effects of flare taper lengths were investigated, and it was discovered that the VSWR improved substantially as the taper length was increased from one-quarter wavelength at the lowest UWB frequency to lengths exceeding one-half wavelength, although decreasing rates of performance gains were apparent in this region. Further, the asymmetry of the inline-balun energy pattern in the E-plane diminished substantially as the flare length increased. As the aperture size grew from one-quarter wavelength at the lowest UWB frequency to one wavelength, it was seen that the E-plane energy pattern asymmetry and VSWR were reduced, although with decreasing rates of performance improvement. Widening or thickening the plates in the flare region had the effect of decreasing the E-plane energy pattern asymmetry. The array behavior of one of the tapered-back elements fed with the inline balun was studied, and the VSWR was shown to remain low for broad angular scanning even with half-wavelength spacing at the highest UWB frequency. It should be noted that additional experiments showed that as the pulse time width became less than the time for electromagnetic energy to traverse the flare arc length, the boresight radiated signal became closer in shape to the replica of the incident voltage and bore less resemblance to the shape of the derivative of the incident voltage. It should also be mentioned that the tapered-back, balun-fed, flared-horn antennas exhibited UWB behavior well above the 12 GHz upper design frequency and slightly below the 4 GHz lower frequency. The upper frequency limit would be determined by the electrical size of both the parallel-plate separation and the antenna discontinuities, while the lower frequency limit could be lowered by lengthening the balun.

REFERENCES

1. K. S. Yee, "Numerical Solution of Initial Boundary Value Problems Involving Maxwell's Equations in Isotropic Media," *IEEE Antennas Propagat.* **14**, 302–307 (May 1966).

2. D. Lamensdorf and L. Susman, "Baseband-Pulse-Antenna Techniques," *IEEE Antennas Propagat. Mag.* **36**(1), 20–30 (Feb. 1994).

3. M. Kragalott and W. Pala, "Inline coaxial balun-fed ultrawideband cornu flared horn antenna," 1999. URL `http://www.google.it/patents/US5973653A`, US Patent 5973653A.

4. K. L. Shlager, G. S. Smith, and J. G. Maloney, "Optimization of Bow-Tie Antennas for Pulse Radiation," *IEEE Antennas Propagat.* **42**(7), 975–982 (July 1994).

5. E. Thiele and A. Taflove, "FD-TD Analysis of Vivaldi Flared Horn Antennas and Arrays," *IEEE Antennas Propagat.* **42**(5), 633–641 (May 1994).

6. R. Luebbers, L. Chen, T. Uno, and S. Adachi, "FDTD Calculation of Radiation Patterns, Impedance, and Gain for a Monopole Antenna on a Conducting Box," *IEEE Antennas Propagat.* **40**(12), 1577–1583 (Dec. 1992).

7. J. G. Maloney, G. S. Smith, and W. R. Scott, "Accurate Computation of the Radiation from Simple Antennas Using the Finite-Difference Time-Domain Method," *IEEE Antennas Propagat.* **38**(7), 1059–1068 (July 1990).

8. R. Janaswamy, "An Accurate Moment Method Model for the Tapered Slot Antenna," *IEEE Antennas Propagat.* **37**(12), 1523–1528 (Dec. 1989).

9. R. Janaswamy and D. Schaubert, "Analysis of the Tapered Slot Antenna," *IEEE Antennas Propagat.* **AP-35**(9), 1058–1065 (Sept. 1987).

10. P. R. Foster, J. D. Halsey, and M. G. M. Hussain, *Ultra-Wideband Antenna Technology* (CRC Press, Inc., Ann Arbor, 1995).

11. R. C. Robertson and M. A. Morgan, "Ultra-Wide-Band Impulse Antenna Study and Prototype Design," Naval Postgraduate School, Deptartment of Electrical and Computer Engineering, Code EC, Monterey, CA 93943, Apr. 1993.

12. J. D. Kraus, *Antennas*, 2nd ed. (McGraw-Hill, New York, 1988).

13. P. J. Gibson, "The Vivaldi antenna," Proceedings of the European Mic. Conf., 1979, pp. 101–105.

14. J. R. Fisk, "Microstrip transmission line," *Ham Radio* pp. 28–37 (Jan. 1978).

15. R. W. Klopfenstein, "A Transmission Taper of Improved Design," *Proc. IRE* **44**, 31–35 (Jan. 1956).

16. J. W. Duncan and V. P. Minerva, "100:1 Bandwidth Balun Transformer," *Proc. IRE* **48**(2), 156–164 (Feb. 1960).

17. P. R. Foster and S. M. Tun, "A Wideband Balun from Coaxial Line to TEM Line," Proceedings of the 9th Inter. Conf. Antennas Propagat. (IEE/URSI/UKRI), Apr. 1995, pp. 286–290.

18. V. A. Kolobov and G. A. Polukhin, "An Ultrabroadband Microwave Antenna," *Telecommun. Radio Eng.* **46**(1), 113–115 (1991).

19. T. P. Montoya and G. S. Smith, "A Comparison of Several Broadband Loaded Monopoles for Pulse Radiation," Proceedings of the IEEE Antennas and Propagation Society International Symposium 1995 (IEEE APS), June 1995, pp. 198–201.

20. J. A. Stratton, *Electromagnetic Theory* (McGraw-Hill, New York, 1941).

21. E. Vollmer and J. H. Hinken, "Synthesis Method for Broad-Band Tapered Wire Antennas and Its Experimental Verification," *IEEE Antennas Propagat.* **37**(8), 959–965 (Aug. 1989).

22. M. J. Poveinelli, "Wideband Dual Polarized Apertures Utilizing Closely Spaced Printed Circuit Flared Slot Antenna Elements for Active Transmit and Receive Array Demonstrations," Proceedings of the 1989 Antenna Applications Symp., Sept. 1989.

23. E. Jahnke and F. Emde, *Tables of Functions*, 4th ed. (Dover Publication, Inc., New York, 1945).

24. R. J. Luebbers, *User's Manual for XFDTD* (REMCOM, Inc., State College, PA 16805, July 1994).

25. D. N. Buechler, D. H. Roper, C. H. Durney, and D. A. Christensen, "Modeling Sources in the FDTD Formulation and their Use in Quantifying Source and Boundary Condition Errors," *IEEE Antennas Propagat.* **43**(4), 810–814 (Apr. 1995).

26. J. P. Berenger, "A perfectly matched layer for the absorption of electromagnetic waves," *J. Comput. Phys.* **14**(3), 185–200 (May 1994).

27. C. E. Reuter, R. M. Joseph, E. T. Thiele, D. S. Katz, and A. Taflove, "Ultrawideband Absorbing Boundary Condition for Termination of Waveguiding Structures in FD-TD Simulations," *IEEE Antennas Propagat.* **4**(10), 344–346 (Oct. 1994).

28. J. D. Cermignari, R. G. Madonna, and P. J. Scheno, "Measurements of the Performance of a Cavity Backed Exponentially Flared TEM Horn," *Ultrawideband Radar SPIE Proceedings* **1631**, 146–154 (Jan. 1992).

29. A. K. Lai, A. L. Sinopoli, and W. D. Burnside, "A Novel Antenna for Ultra-Wide-Band Applications," *IEEE Antennas Propagat.* **40**(7), 755–760 (July 1992).